Article

Microstructure and Mechanical Property of Compact Graphite/6061Al Composite Prepared by Ultra-High Pressure Sintering

Changyun Li [1,2], Yasong Wang [2], Lei Xu [1,2,*], Yang Liu [2], Ningning Lu [2] and Guofa Mi [2,*]

[1] Faculty of Engineering, China University of Petroleum-Beijing at Karamay, Karamay 834000, China; lucy1226@126.com

[2] School of Materials Science and Engineering, Henan Polytechnic University, Jiaozuo 454000, China; 211706020012@home.hpu.edu.cn (Y.W.); 211806020028@home.hpu.edu.cn (Y.L.); lnn18236881599@163.com (N.L.)

* Correspondence: xulei_80@126.com (L.X.); peter@hpu.edu.cn (G.M.)

check for updates

Abstract: Graphite/6061 aluminum (G/6061Al) composites with different content of graphite were ultra-high pressure (UHP)-sintered and hot pressing (HP)-sintered, respectively. The result shows that homogeneous dispersion of graphite flakes in the 6061Al matrix can be achieved using graphite flakes coated by nano-Al particles, both in the UHP-sintered and in the HP-sintered composite. Due to the comprehensive effects of ultra-high pressure, high temperature and formation of Al_4C_3, the UHP-sintered composites endowed with higher relative density, higher hardness, stronger tensile strength and better wear resistance than the HP-sintered composite. The highest tensile strength of the UHP-sintered with 5 vol.% graphite is 183 MPa. Wear test reveals that the wear rate of the UHP sintered with 10 vol.% G/6061Al decreases drastically when the sintering temperature is 650 °C or higher, which is one to three orders of magnitude lower than that of the HP-sintered. The lowest wear rate of the UHP sintered with 10 vol.% graphite is 0.15×10^{-5} g/mm, while that of the HP-sintered composite is 133×10^{-5} g/mm.

Keywords: ultra-high pressure sintering; graphite/6061Al composite; relative density; tensile strength; wear rate

1. Introduction

Graphite-aluminum composites (G/Al) present good machinability [1], self-lubrication [1] and low friction coefficient [2], good friction and wear resistance [2,3], improved mechanical properties [4], high specific strength and high specific rigidity [5,6], as well as low thermal expansion and high damping capacity [7]. These characteristics provide potential applications of the G/Al, especially in the fields where excellent mechanical properties and wear resistance are required.

In the past decades, preparation of the G/Al attracted considerable attention. As is known, graphite is easy to float in molten aluminum and the wettability between graphite and Al or Al alloy is very low [8], which increases the tendency of inhomogeneous distribution of graphite and of the formation of porosity at the interface of graphite and the matrix. Keeping the aluminum matrix solid during preparation (powder metallurgy, including pressure-free sintering [9,10], hot pressing sintering [11–14], spark plasma sintering [7,15], electrical resistance heat assisted pressing [16]) may reduce these defects and provide more superior performances. However, there are still porosities formed during the powder metallurgy process, which has a detrimental effect on the property [17,18]. Researchers believe it is important to decrease the porosity and increase the relative density, which can be achieved by using coated graphite [15], hot deforming after sintering [9], optimizing sintering

temperature [7] and sintering under pressure [19]. The last two are important sintering parameters that have been verified to have a great influence on relative density. Durowoju [7] reported that relative density was raised from 89.5% to 97.1% when sintering temperature was optimized. The literature [14] documented that the relative density was higher than 97% when sintering at a high temperature (500 °C) and high loading (150 MPa). Fallahdoost [3] reported that the relative density higher than 99% could be generated by sintering at 500 MPa. It seemed that both the sintering temperature and the sintering pressure were helpful for densification, but not enough attention was focused on the G/Al sintered at a high load and the consequent properties. Furthermore, the mechanical performances of the G/Al composites still need to be improved, although high relative density was obtained in previous investigations [3,5,9].

Thus, preparation of the graphite-aluminum alloy composite by using ultra-high pressure (UHP) sintering at pressure of 5.2 GPa was investigated in order to achieve the compact composite and its consequent excellent properties. Considering that the properties of the composite could be further improved by heat treatment in later application, the commonly used 6061Al was chosen to be the matrix because of its good comprehensive performance, good formability and good heat treatability. To obtain homogeneous dispersion of graphite in the composite, graphite flakes coated with nano-aluminum (NAGF) powders were used. Correspondingly, microstructure, relative density, hardness, tensile strength and wear resistance of the compact graphite-6061Al composite (G/6061Al) were investigated and compared with that of the G/6061Al hot pressing (HP)- sintered.

2. Materials and Methods

Spherical 6061Al powders with the diameter range of 16 μm to 86 μm, gas-atomized by JW-25 vacuum metal atomization furnace, were used as the matrix. To reduce the agglomeration of graphite, NAGF powders were used that were prepared by pre-coating commercial irregular graphite flakes (diameter range of 20 μm–70 μm and average thickness of about 3 μm), with nano-Al powders (average diameter of 80 nm, purity of 99%, purchased from Jiaozuo Ban-Lv Nano. Eng. Co. Ltd.). The detailed process of pre-coating is described in our earlier works [13].

The 6061Al and NAGF powders with graphite content of 0 vol.%, 5 vol.%, 10 vol.% and 15 vol.% were respectively mixed in QM-3A mill for 30 min at a rotation rate of 1400 r/min. The blended powders were put into a mold, assembled by pyrophyllite bulk embedded with a dolomite tube, a NaCl tube and a graphite tube. Then, the mold was dried and put into a 6MK-3WY-60 cubic hinge presser, in which the UHP sintering was performed for 40 min at a pressure of 5.2 GPa and temperature of 450 °C, 550 °C, 650 °C and 750 °C, respectively. To analyze the improvement of the sintering pressure on the properties, G/6061Al bearing 0 vol.%, 5 vol.% and 10 vol.% graphite were also HP-sintered at 35 MPa and temperature of 520 °C. Both of the two sintering processes were performed in avacuum atmosphere lower than 1.3×10^{-3} Pa.

The relative density was the ratio of practical density vs theoretical density. The practical density was measured by a wax-coated method, based on the principle of Archimedes. The theoretical density ρ_T (g/cm^3) was calculated according to Formula (1):

$$\rho_T = V_{Al}\rho_{Al} + V_G\rho_G \qquad (1)$$

where ρ_{Al} and ρ_G are theoretical densities of 6061Al andgraphite (g/cm^3); V_{Al} and V_G are volume fractions of 6061Al and graphite (cm^3). The HRA hardness of the as-pressed sample was measured by Electric Rockwell hardness tester (500MRA) with a diamond cone indenter, at a load of 60 kgf and dwell time of 10 s. In order to evaluate the tensile property, the sintered composite was machined to specimens with a gauge section size of 2.5 mm-long, 1.4mm-wide and 1mm-thick. The specimens were tested by Instron 5848 tensile tester at a tensile rate of 0.15 mm/min. A dry sliding test was carried out on MMW-1 vertical universal friction and a wear testing machine, under the load of 20 N and rotation speed of 240 r/min for about 900 s (distance of about 135,000 mm). The samples for the test

were machined to 12.7 mm length and 4.8 mm diameter. The sample was weighed before and after the dry sliding test and the weight loss was obtained. The wear rate of the composite was evaluated by the ratio of the weight lost to the dry sliding distance.

The morphology of the powder, microstructure of the composite, fracture surfaces of tensile samples and worn surfaces of wear samples were observed by OLYMPUS GX51 optical microscope, field emission scanning electron microscopy (SEM; FEI Quanta 250 FEG; ZEISS Sigma 300) and transmission electron microscope (High Resolution TEM, JEM-2100). The distribution of Al, C and O was investigated by means of energy dispersive spectroscopy (EDS). Phase analysis of the composite was carried out by X-ray diffractometer (Smart-lab, Rigaku, Japan), at 40 kV and 200 mA and using CuKα radiation (λ = 0.15406 nm), within 2θ = 20°–85°, at scanning speed of 10°/min.

3. Results and Discussion

3.1. Morphology of the Powder

Morphologies of the nano-Al powders, graphite flakes, NAGF and the mixed composite powders are presented in Figure 1. The raw nano-Al powders are easy to be agglomerated and the raw graphite flakes are obviously irregular, shown in Figure 1a,b. It can be seen from Figure 1c that the agglomeration of the nano-Al powders was distinctly broken up, conversely adhering to graphite flakes, during the pre-coating process. Then, the graphite flakes were completely or partly coated by nano-Al powders, which were propitious for improving dispersion uniformity of graphite in the subsequent mixing process, shown in Figure 1d.
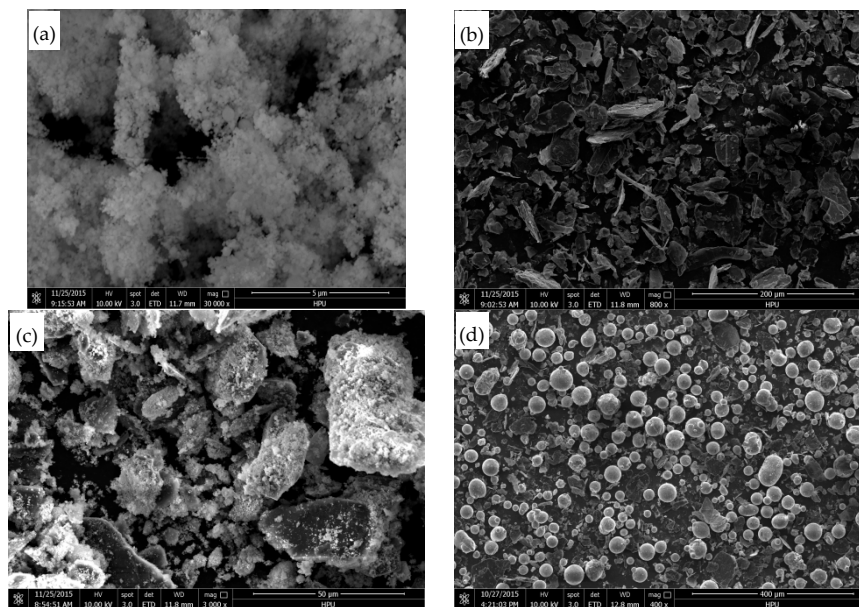

Figure 1. Scanning electron microscopy (SEM) micrographs of (**a**) nano-Al powders, (**b**) graphite flakes, (**c**) graphite flakes coated with nano-aluminum (NAGF) powders and (**d**) the mixed composite powders with graphite content of 10 vol.%.

3.2. Microstructure, Relative Density and Phase Analysis of the G/6061Al Composite

The microstructure of the UHP-sintered G/6061Al consists of Al matrix (light region) and graphite (dark region), with graphite flakes uniformly distributing in the Al matrix, which signifies the effect of pre-coating on scattering the graphite flakes, shown in Figure 2. It is observed in the optical images that no significant difference has been caused by variation of the sintering temperature, seen from Figure 2b,d. However, some agglomerations appear when the graphite content increased to 15 vol.%, as shown in Figure 2c. Due to the limited magnification, no pores are found in the optical microcopies, shown in Figure 2. However, the relative density is measured to be only 91.35%, implying the existence

of pores in the G/6061Al HP-sintered at 35 MPa and 520 °C; meanwhile, the relative density of the G/6061Al with 10 vol.% graphite, sintered at 5.2 GPa and 450 °C, is 98.5% and is the lowest among the UHP-sintered, seen in Figure 3a,b.
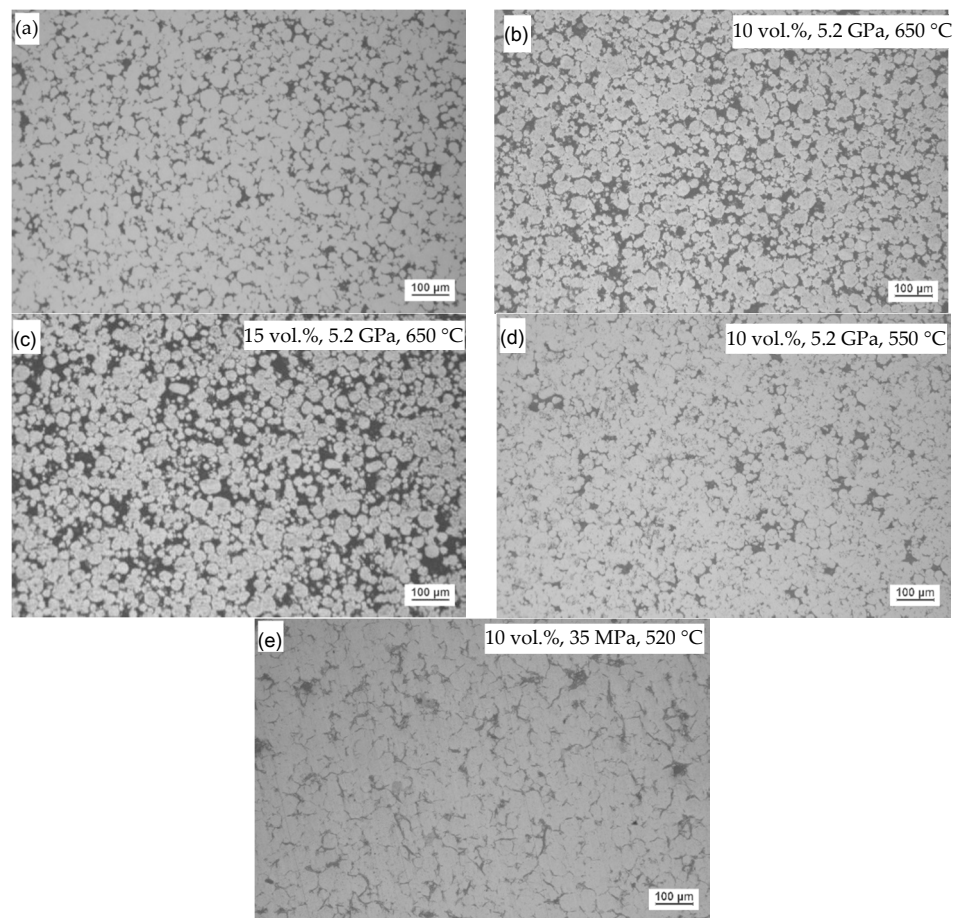

Figure 2. Optical images of the sintered G/6061Al with (**a**) 5 vol.%, (**b**) 10 vol.% and (**c**) 15 vol.% graphite at 5.2 GPa and 650 °C and (**d**) that with 10 vol.% at 5.2 GPa and 550 °C, or (**e**) at 35 MPa and 520 °C.
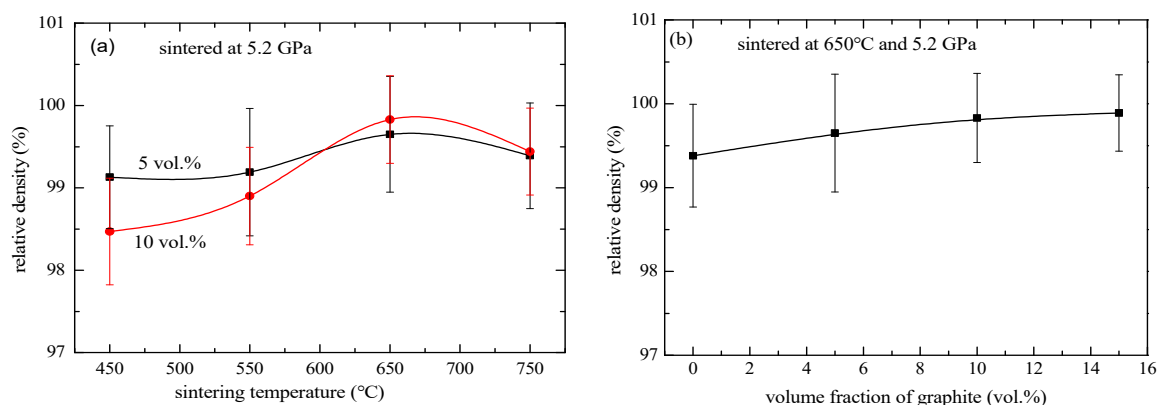

Figure 3. Effect of (**a**) sintering temperature and (**b**) graphite content on the relative density of the G/6061Al.

It is also illustrated in Figure 3a that the relative density increases when raising the temperature from 450 °C to 650 °C, but slightly decreases as the sintering temperature is raised to 750 °C at 5.2 GPa. When the temperature is not higher than 550 °C, the relative density of the composite bearing 5 vol.% graphite is higher than that bearing 10 vol.% graphite, while an inverse result is presented when the

sintering temperature is higher than 550 °C, shown in Figure 3a. In addition, it is also observed that adding more graphite increases the relative density when the G/6061Al is sintered at 5.2 GPa and 650 °C, as shown in Figure 3b. It is reported that the relative density of G/Al decreases with the increase of graphite [9,12–14], different from the above result, which is considered to probably be caused by the reaction of Al and graphite during the UHP sintering at a high temperature.

More precise observations were carried out by SEM that demonstrate some pores existing in the HP-sintered, marked by a white arrow in Figure 4a, but pores are still scarcely observed in the UHP-sintered G/6061Al, shown in Figure 4b–d. Furthermore, the shape of graphite in the UHP-sintered G/6061Al is changed to be quite different from its original. During the UHP sintering, relative movement between graphite and 6061Al matrix was constricted by the hydrostatic pressure, correspondingly the graphite appearance depended on the shape of the gap between 6061Al particles. Under the ultra-high pressure, the 6061Al particle was also deformed and could not keep its original spherical shape, leading to flat boundaries at the parts contacting with graphite, similar to that of stable grain boundaries. At the sites contacting with other 6061Al particles, the original surface disappeared and the two Al particles combined with each other, shown in Figure 4b–d. Concurrently, the gaps between the 6061Al particles were substantially reducedand the pores at the interface of the original graphite flake and the 6061Al particle could also be eliminated by the ultra-high pressure, leading to a high relative density. For instance, Figure 3a shows that relative densities of 5 vol.% and 10 vol.% graphite G/6061Al are 99.19% and 98.9% individually, sintered at 550 °C and 5.2 GPa.
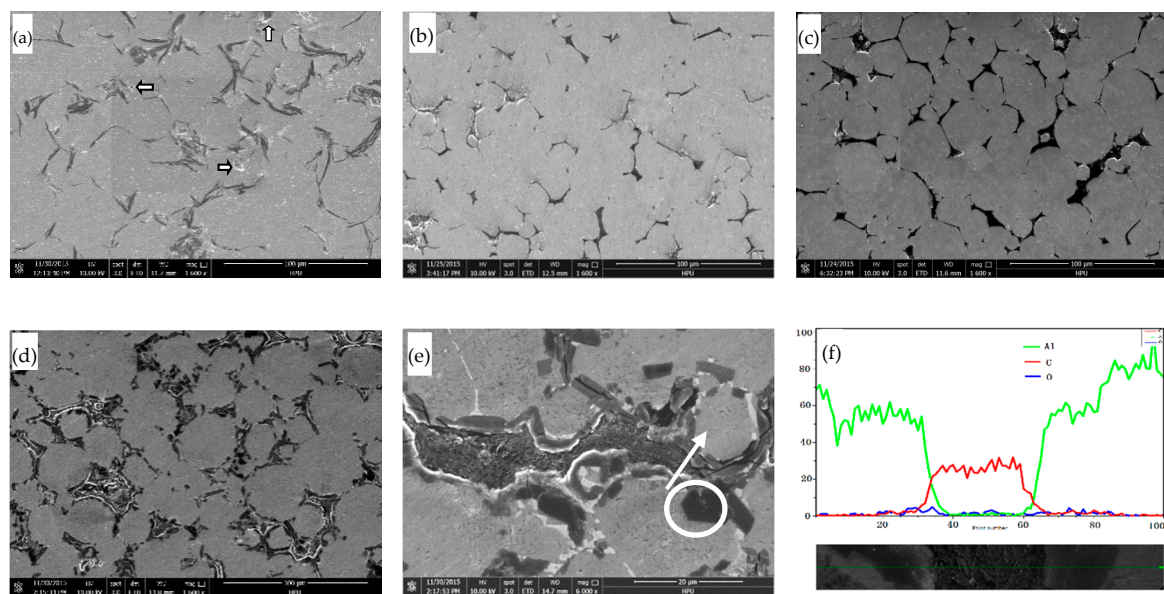

Figure 4. SEM micrograph of the composite (**b**) with 5 vol.% graphite sintered at 5.2 GPa and 550 °C and of that with 10 vol.% graphite under (**a**) 35 MPa and 520 °C, or (**c**) 5.2 GPa and 550 °C, (**d,e**) 5.2 GPa and 650 °C, and (**f**) EDS line scanning along the arrow in (**e**).

In order to determine the interfacial reaction between the graphite and 6061Al matrix, an observation was performed. The result shows that the interface is not clear when the temperature is raised to 650 °C, while there are many gray areas around the interface, some of which present to be regular shapes such as bar-type and hexagon, shown as region 1 in Figure 4e. Line scanning revealed that the regions appeared in the 6061Al matrix on both sides of the graphite, consisting of C and Al, implying that Al_4C_3 phase was formed. Figure 5 also demonstrates the formation of bar-type and hexagon Al_4C_3 and nano-Al_4C_3 in the G/6061Al composite UHP sintered at 650 °C. However, UHP sintered at a temperature of 550 °C or below, the XRD pattern distinctly manifests that no Al_4C_3 is visible, despite the content of graphite, as can be seen in Figure 6. It has been reported [10,20] that Al_4C_3 exists in Al7075-graphite composites sintered at 550 °C and hot extruded at 500 °C and the

effect of graphite on the formation of Al_4C_3 is deemed to be significant, in consistent with our finding. The reason is that the sintering temperature can seriously affect the formation of Al_4C_3 and the UHP can also impede the formation of Al_4C_3 to a certain extent. When the sintering temperature is 650 °C or higher, the XRD intensity of carbon is evidently decreased, while that of Al_4C_3 is increased, shown in Figure 6. This variation also means that the addition of graphite may motivate the reaction of graphite and Al, leading to the formation of Al_4C_3 at a high sintering temperature.
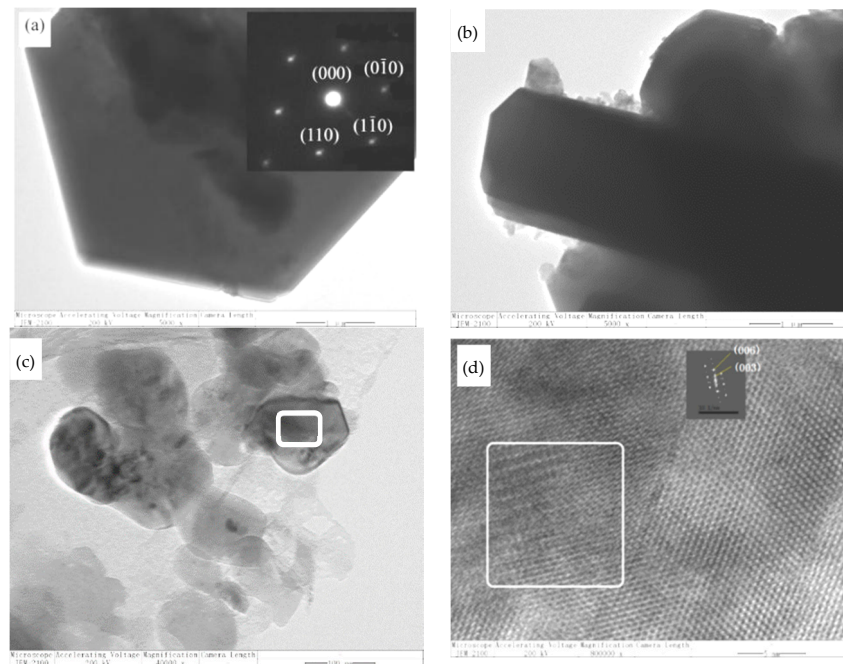

Figure 5. HRTEM micrographs of (**a**) hexagon or (**b**) bar-type and (**c**) nano-Al_4C_3, and (**d**) selected area electron diffraction of (**c**).
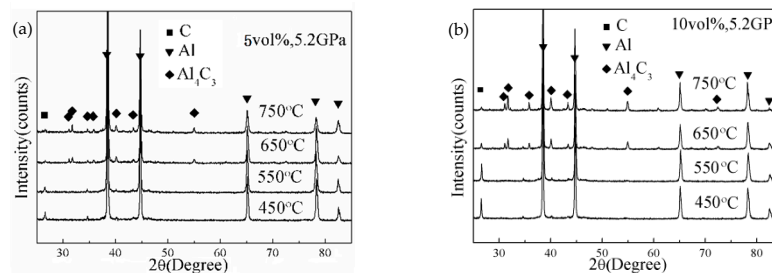

Figure 6. XRD patterns of the sintered with G content of (**a**) 5 vol.% and (**b**) 10 vol.%, at different temperatures under 5.2 GPa.

At a high sintering temperature, the diffusion of elements and the combination between the graphite and Al matrix were also improved, thus porosities were easy to be reduced. Furthermore, the interplanar distance and lattice constants of Al and Al_4C_3 were able to be decreased by the ultra-high pressure [21,22], which was instrumental in improving relative density. Therefore, it is concluded that the high relative density of the UHP-sintered G/6061Al should be attributed to the ultra-high sintering pressure and the high sintering temperature.

3.3. Mechanical Properties of G/6061Al Composite

The effect of the sintering temperature and the content of graphite on hardness is shown in Figure 7a,b. During hardness testing, it was found that the hardness of HP-sintered 5 vol.% G/6061Al was HBS 39.3—too soft to be measured by an HRA tester, while the UHP-sintered G/6061Al was much

harder. Figure 7a,b presents that the hardness of the UHP-sintered G/6061Al increases with the increase of graphite and with raising the sintering temperature. Figure 7a also illustrates that the hardness of the 10 vol.% is lower than that of the 5 vol.% at sintering temperature lower than 650 °C, while it is the opposite at sintering temperature of 650 °C or higher, similar to the comparison of relative density in Figure 3a. Based on the foresaid microstructure analysis, it is obviously caused by the formation of Al_4C_3 and relative density.
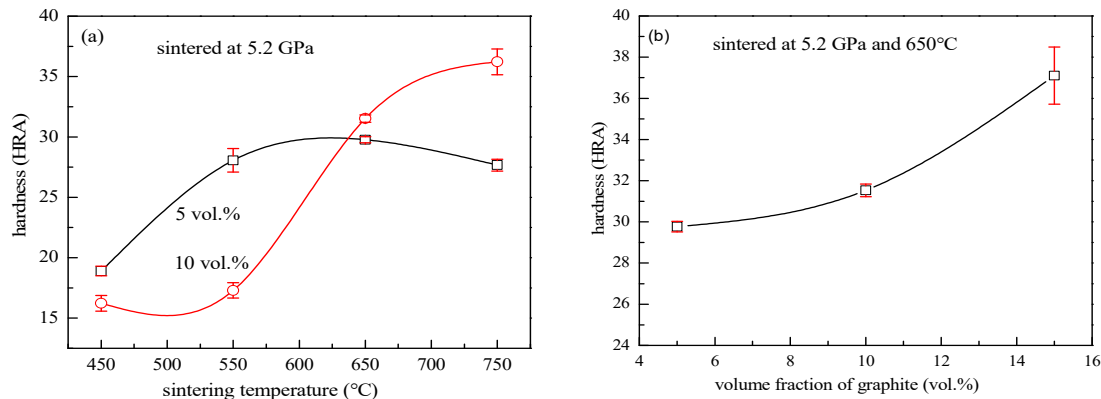

Figure 7. Effect of (**a**) sintering temperature and (**b**) graphite content on the hardness of the G/6061Al.

Table 1 lists out the tensile strengths of the G/6061Al composites in this investigation and other reported. Table 1 shows that the tensile strength of the UHP-sintered 6061Al with 0 vol.% graphite is 338 MPa, equivalent to the tensile strength of the 6061Al after T6 heat treatment; the tensile strength of the HP-sintered 6061Al is only 179 MPa, much lower than the UHP-sintered 6061Al. With the addition of 5 vol.% G, the tensile strengths of the UHP-sintered and HP-sintered G/6061Al decreased. However, the tensile strength of the UHP-sintered 5 vol.% G/6061Al is 183 MPa, slightly higher than the HP-sintered 6061Al, and about two times of the HP-sintered 5 vol.% G/6061Al.It is evident that the strength of the HP-sintered is much lower than that of the UHP-sintered, but is comparable to that of the reported [2,5,9]. This can also demonstrate that the ultra-high pressure has an important effect on promotion of strength of the G/6061Al.

Table 1. Tensile strengths of the composites in this investigation and other reported literature.

Processing Parameters	Yield Strength $Rp_{0.2}$ (MPa)	Tensile Strength Rm (MPa)
5.2 GPa, 650 °C, 0 vol.% G	293	338
5.2 GPa, 650 °C, 5 vol.%G	142	183
35 MPa, 520 °C, 0 vol.% G	81	179
35 MPa, 520 °C, 5 vol.% G	74	77
6101Al, casting + T6 heat treatment [2]	-	164
0 wt.% G/6016Al, sintering + hotextruding [9]	75	106
5 wt.% G/6016Al, sintering + hot extruding [9]	67 (Measured from the curve)	97 (Measured from the curve)
2 wt.% Graphene [5]	48	94
2 wt.% Graphite [5]	44	75.5

An investigation of fracture surface shows big dimples in the fracture surface of the 0 vol.% G/6061Al sintered at 5.2 GPa, which generally represents ductile fracture, as shown in Figure 8a. However,the dimpleis alike to grain boundary, meaning that the interface boundary between the Al particles is still the weak region, which can act as the crack source and the crack propagation path. It is deemed that 6061Al particles were extruded together with small relative slippage under high isostatic pressure and thesurface impurities of oxidation were retained in part of the interface. Accordingly, the bonding strength at interface was lower than that at the interior, thus the interfaceacted as the crack source and the propagation path. Though graphite could promote the slither of 6061Al powders during the UHP sintering, which was propitious to destroy the oxide layer and improved the connection

between particles, graphite could also be the source of the crack. Therefore, partial ductility fracture was formed during the tensile process of the UHP-sintered 5 vol.% G/6061Al, shown in Figure 8c.
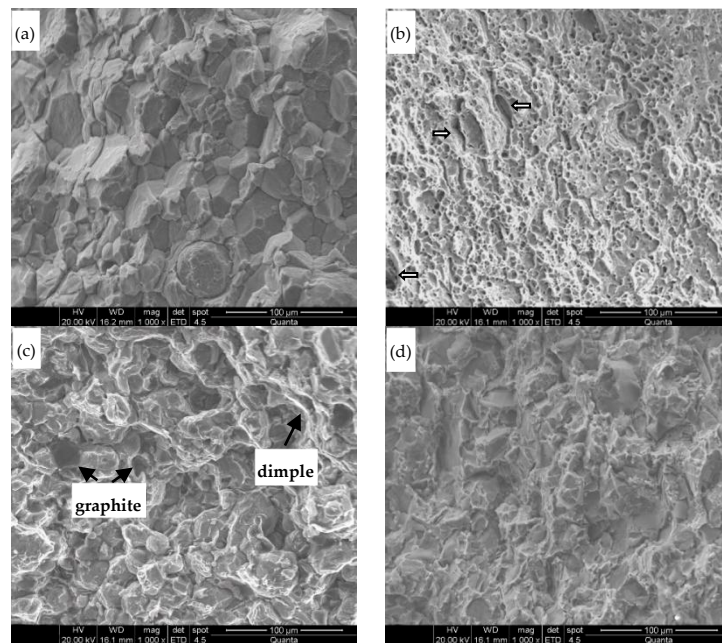

Figure 8. Fracture surfaces of (**a**,**b**) the 0 vol.% UHP and HP-sintered, and (**c**,**d**) that of the 5 vol.% G/6061Al corresponding.

During the HP sintering, a relatively larger glide between the particles was generated and made the oxide layer easy to be broken, which brought about good integration of particles. Thereby, it presents characteristics of a typical ductile fracture in the fracture surface of the HP-sintered 0 vol.% G/6061Al. As is shown in Figure 8b, there are many small dimples in the fracture surface. But there are some pores, shown by the arrows in Figure 8b, which can act as the crack initiation position. With addition of 5 vol.% graphite, the ductility is further decreased, caused by the brittleness and low strength of graphite and existence of pores. Consequently, a mixture of brittle and ductility fracture is formed in the HP sintered 5 vol.% G/6061Al, shown in Figure 8d.

3.4. Wear Resistance of G/6061Al Composite

Table 2 lists out the friction coefficient and the wear rate of G/6061Al bearing 10 vol.% graphite. Figure 9 shows the SEM micrograph of the worn surface and EDS elemental maps of the regions marked by a white box in the worn surface.

Table 2. Friction coefficients and wear rates of the G/6061Al with 10 vol.% graphite.

Processing Parameters	UHP Sinteredat 5.2 GPa				HP Sinteredat 35 MPa and 520 °C
	450 °C	550 °C	650 °C	750 °C	
Friction coefficient	0.484	0.483	0.595	0.544	0.455
Wear rate (10^{-5} g/mm)	12.45	17.92	0.97	0.15	133.89

Table 2 manifests that wear rate of the HP sintered is the highest and that of the UHP-sintered is about one to three orders of magnitude lower. When the sintering temperature is raised from 450 °C to 550 °C at 5.2 GPa, the wear rate is increased from 12.45×10^{-5} g/mm to 17.92×10^{-5} g/mm. Raising the sintering temperature to 650 °C or higher, the wear rate of the UHP-sintered is substantially decreased, listed in Table 2. For example, the wear rate of the UHP sintered at 750 °C is 0.15×10^{-5} g/mm,

which is only about 1% of that at 550 °C. In addition, it is also shown that the wear resistance of the UHP-sintered is proportional to its hardness.

SEM observation shows that plastic deformation of 6061Al exists on the worn surface during the wear test, seen in Figure 9. As wear progresses, partly adhesive delamination of the deformed 6061Al layer occurs on the surface, which is the mark of adhesion wear. There are also grooves, spalling pits and wear debris on the worn surfaces, marking the abrasion wear. Figure 9a also shows that the delamination is serious on the worn surface of the UHP sintered at 550 °C and 5.2 GPa. With the elevation of the sintering temperature, the composite presents better resistance to delamination and spalling, shown in Figure 9b. The reason is that the G/6061Al is more compact and harder (partly caused by Al_4C_3) when it is UHP-sintered at a temperature of 650 °C or 750 °C. It is also evident that the delamination is the main factor of weight loss of the UHP-sintered.
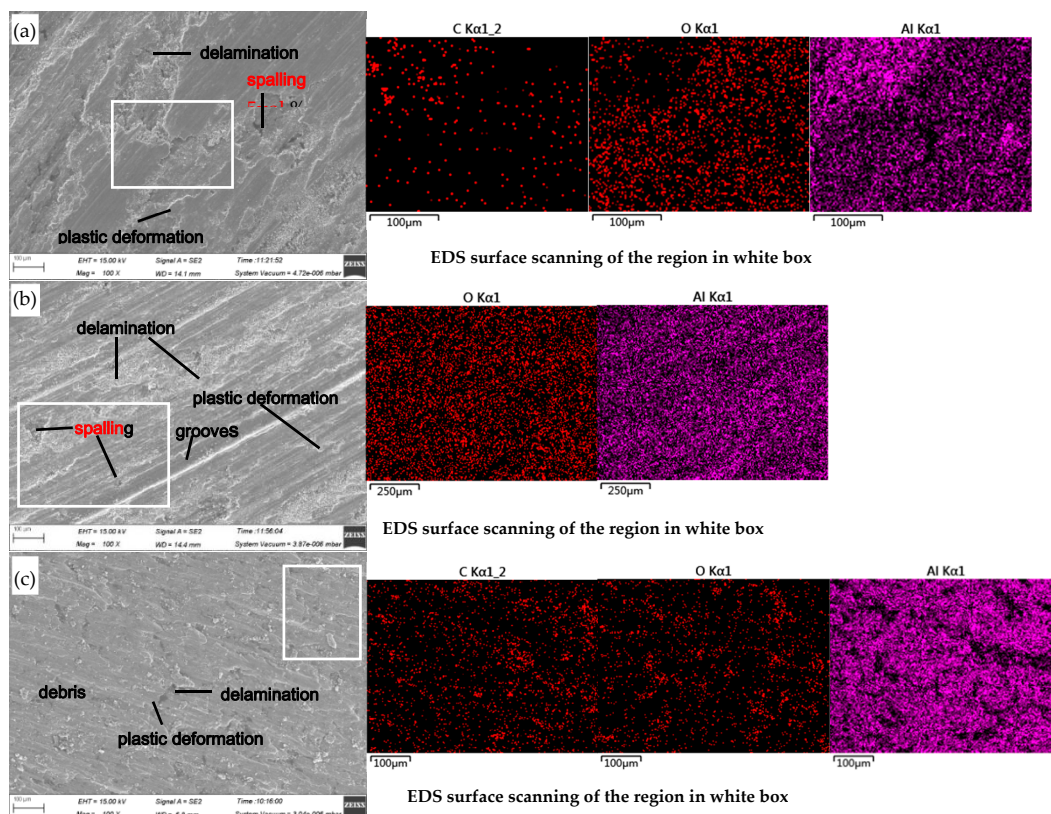

Figure 9. SEM micrographs and EDS surface scanning results of worn surfaces of the composites bearing 10 vol.% graphite sintered at (**a**) 5.2 GPa and 550 °C, (**b**) 5.2 GPa and 750 °C and (**c**) 35 MPa and 520 °C, respectively.

Table 2 also exhibits that the friction coefficients are lower, but the wear rates are much higher when the 10 vol.% G/6061Al composite is respectively HP-sintered and UHP-sintered at a temperature not higher than 550 °C. Elemental map provides that there is graphite distributed on the worn surface of the UHP sintered at a low temperature and the HP-sintered, seen in Figure 9b,c. Furthermore, a large amount of uniform graphite is found on the worn surface of the HP-sintered, of which the relative density is very low, shown in Section 3.2. Then, it can be induced that the lower the density of the composite, the easier the graphite will fall off and the better the lubrication will be. However, it is not that the lower the friction coefficient, the lower the wear rate. The relative density and hardness also have a great influence on the wear rate. The literature [3] also reported a similar law, in which TiC particles were considered to act as reinforcement in the Al/TiC/graphite composite and increase the wear resistance of the Al/TiC/graphite composite.

Elemental map presents that there is no carbon found on the worn surface of the composite UHP sintered at 5.2 GPa and 750 °C, seen in Figure 9b. This is because most of the graphite reacted with Al to form Al_4C_3 at 750 °C and the composite is more compact than that UHP sintered at 550 °C, shown from Figures 3a and 7b. In addition, Figure 9b exhibits that a large amount of oxygen is found on the worn surface. SEM observation also shows thata lot of tiny aluminum oxide particles adhered to the worn surfaces, especially on that of the UHP sintered at 650 °C and 5.2 GPa, as observed in Figure 9. It can be induced that aluminum oxide should be formed at the interface of the G/6061Al and the counter plate, as the temperature rise caused by friction heating during the wear test. Researchers believe that the aluminum oxide could act as a solid lubricant that prevents the rubbing surfaces being indirect contact and considerably reduce the wear loss [6].

Thus, it can be summarized that the wear resistance of the G/6061Al can be enhanced by its higher relative density and higher hardness, resulted from the ultra-high pressure and formation of Al_4C_3. In the HP-sintered, graphite is favorable to fall off and lubricate, which cannot effectively improve the wear resistance. It is not just graphite—aluminum oxide may also act as the lubricant to reduce the wear loss of the G/6061Al UHP sintered at a high temperature.

4. Conclusions

Compact G/6061Al composites were fabricated by UHP sintering at different sintering temperatures, using NAGF powders. Homogeneous dispersion of graphite in the G/6061Al with a content of graphite no higher than 10 vol.% can be achieved by UHP sintering; but slight agglomeration of graphite will be formed with the addition elevated to 15 vol.%. Compared with the HP sintered, the UHP sintered G/6061Al composite has higher relative density, higher hardness, stronger tensile strength and better wear resistance. The highest relative density of the 10 vol.% G/6061Al UHP sintered is 99.8%—much higher than that of the HP sintered at 35 MPa, which is only about 91.35%. The relative density and hardness of the UHP sintered at 650 °C or higher increases with the rise of graphite content, which is comprehensively caused by the compaction of high pressure, better combination of graphite and Al matrix, and formation of Al_4C_3. Due to the high density and hardness, the lowest wear rate of the UHP sintered 10 vol.% G/6061Al composite is 0.15×10^{-5} g/mm—about three orders of magnitude lower than that of the HP sintered. Furthermore, the wear rate of the UHP sintered decreases drastically when the sintering temperature is raised to 650 °C or higher. These results demonstrate that elevation of sintering pressure is advantageous to prepare dense G/6061Al composites and to achieve good mechanical properties. It is also deemed that the mechanical properties of the G/6061Al composites can be further improved if heat treatment is combined to enhance the properties of the 6061Al matrix.

Author Contributions: C.L. contributed to the conceptualization and methodology of the study; Y.W. performed part of the experiment and wrote the original draft; L.X. contributed significantly to analysis and manuscript preparation; Y.L. performed the data analyses; N.L. performed the experiment; G.M. helped perform the analysis with constructive discussions. All authors have read and agreed to the published version of the manuscript.

Conflicts of Interest: The authors declare no conflicts of interest.

References

1. Omrani, E.; Moghadam, A.D.; Menezes, P.L.; Rohatgi, P.K. Influences of graphite reinforcement on the tribological properties of self-lubricating aluminum matrix composites for green tribology, sustainability, and energy efficiency—A review. *Int. J. Adv. Manuf. Technol.* **2015**, *83*, 325–346. [CrossRef]
2. Sharma, P.; Paliwal, K.; Garg, R.K.; Sharma, S.; Khanduja, D. A study on wear behaviour of Al/6101/graphite composites. *J. Asian Ceram. Soc.* **2017**, *5*, 42–48. [CrossRef]
3. Fallahdoost, H.; Nouri, A.; Azimi, A. Dual functions of TiC nanoparticles on tribological performance of Al/graphite composites. *J. Phys. Chem. Solids* **2016**, *93*, 137–144. [CrossRef]

4.   Latief, F.; Sherif, E.-S.M. Effects of sintering temperature and graphite addition on the mechanical properties of aluminum. *J. Ind. Eng. Chem.* **2012**, *18*, 2129–2134. [CrossRef]

5.   Yolshina, L.A.; Muradymov, R.V.; Korsun, I.V.; Yakovlev, G.A.; Smirnov, S.V. Novel aluminum-graphene and aluminum-graphite metalliccomposite materials: Synthesis and properties. *J. Alloy. Compd.* **2016**, *663*, 449–459. [CrossRef]

6.   Alam, S.N.; Kumar, L. Mechanical properties of aluminium based metal matrix composites reinforced with graphite nanoplatelets. *Mater. Sci. Eng. A* **2016**, *667*, 16–32. [CrossRef]

7.   Durowoju, M.; Sadiku, E.; Diouf, S.; Shongwe, M.; Olubambi, P. Spark plasma sintering of graphite–aluminum powder reinforced with SiC/Si particles. *Powder Technol.* **2015**, *284*, 504–513. [CrossRef]

8.   Landry, K.; Kalogeropoulou, S.; Eustathopoulos, N. Wettability of carbon by aluminumand aluminum alloys. *Mater. Sci. Eng. A* **1998**, *254*, 99–111. [CrossRef]

9.   Seleman, M.M.E.-S.; Ahmed, M.; Ataia, S. Microstructure and mechanical properties of hot extruded 6016 aluminum alloy/graphite composites. *J. Mater. Sci. Technol.* **2018**, *34*, 1580–1591. [CrossRef]

10.   Deaquino-Lara, R.; Gutiérrez-Castañeda, E.; Estrada-Guel, I.; Hinojosa-Ruiz, G.; García-Sánchez, E.; Herrera-Ramírez, J.M.; Pérez-Bustamante, R.; Martínez-Sánchez, R. Structural characterization of aluminium alloy 7075-graphitecomposites fabricated by mechanical alloying and hot extrusion. *Mater. Des.* **2014**, *53*, 1104–1111. [CrossRef]

11.   Chen, J.-K.; Huang, I. Thermal properties of aluminum–graphite composites by powder metallurgy. *Compos. Part B Eng.* **2013**, *44*, 698–703. [CrossRef]

12.   Kurita, H.; Miyazaki, T.; Kawasaki, A.; Lu, Y.; Silvain, J. Interfacial microstructure of graphite flake reinforced aluminum matrixcomposites fabricated via hot pressing. *Compos. Part A* **2015**, *73*, 125–131. [CrossRef]

13.   Ningning, L.; Lei, X.; Changyun, L.; Youchao, W.; Guofa, M.; Erkuo, Y. Reach of the preparation, microstructure and properties of Gr/6061Al composites sintered by hot pressing sintering. *Rare Met. Mater. Eng.* **2019**, *48*, 1961–1968.

14.   Esmati, M.; Shari, H.; Raeissi, M.; Atrian, A.; Rajaee, A. Investigation into thermal expansion coefficient, thermal conductivityand thermal stability of Al-graphite composite prepared by powder metallurgy. *J. Alloys Compd.* **2019**, *773*, 503–510. [CrossRef]

15.   Tan, H.; Wang, S.; Cheng, J.; Zhu, S.; Yu, Y.; Qiao, Z.; Yang, J. Tribological properties of Al-20Si-5Fe-2Ni-Graphitesolid-lubricating composites. *Tribol. Int.* **2018**, *121*, 214–222. [CrossRef]

16.   Sahoo, B.; Kumar, R.; Joseph, J.; Sharma, A.; Paul, J. Preparation of aluminium 6063-graphite surface composites by anelectrical resistance heat assisted pressing technique. *Surf. Coat. Technol.* **2017**, *309*, 563–572. [CrossRef]

17.   Dolata-Grosz, A.; Śleziona, J.; Formanek, B. Structure and properties of aluminium cast compositesstrengthened by dispersion phases. *J. Mater. Process. Technol.* **2006**, *175*, 192–197. [CrossRef]

18.   Olmos, L.; Martin, C.; Bouvard, D. Sintering of mixtures of powders: Experiments and modelling. *Powder Technol.* **2009**, *190*, 134–140. [CrossRef]

19.   Hafizpour, H.R.; Simchi, A. Investigation on compressibility of Al–SiC composite powders. *Powder Met.* **2008**, *51*, 217–223. [CrossRef]

20.   Deaquino-Lara, R.; Estrada-Guel, I.; Hinojosa-Ruiz, G.; Flores-Campos, R.; Herrera-Ramirez, J.; Martínez-Sánchez, R. Synthesis of aluminum alloy 7075-graphite composites by milling processes and hot extrusion. *J. Alloys Compd.* **2011**, *509*, S284–S289. [CrossRef]

21.   Rong-de, L.; Xiu-sheng, C.; Ying-dong, Q.; Yao, X.; Run-xia, L.; Chan, T. Effect of super high pressure on crystal structure and microstructure of ZA27 alloy. *Chin. J. Nonferrous Met.* **2009**, *9*, 1570–1574.

22.   Solozhenko, V.L.; Kurakevych, O.O. Equation of state of aluminum carbide Al_4C_3. *Solid State Commun.* **2005**, *133*, 385–388. [CrossRef]